CoCO2

Prototype system for a Copernicus CO_2 service

The representation of CO2M satellite retrieval uncertainty in inverse modelling

Eleftherios Ioannidis and Sander Houweling (VUA), Julia

Marshall and Friedemann Reum (DLR), Gregoire

Broquet, Elise Potier and Antoine Berchet (CEA/LISA)

coco2-project.eu

CoCO2

Prototype system for a Copernicus CO_2 service

D5.4 The representation of CO2M satellite retrieval uncertainty in inverse modelling

Dissemination Level: Public

Author(s): E.Ioannidis and S. Houweling (VUA), Julia Marshall, Friedemann Reum (DLR), Elise Potier (CEA, now at LISA), Antoine Berchet (CEA), Gregoire Broquet (CEA)

Date:	27/12/2023
Version:	1
Contractual Delivery Date:	1/10/2023
Work Package/ Task:	WP5/ T5.4
Document Owner:	VUA
Contributors:	Organisations
Status:	for Review

CoCO2: Prototype system for a Copernicus CO_2 service

Coordination and Support Action (CSA)
H2020-IBA-SPACE-CHE2-2019 Copernicus evolution – Research activities in support of a European operational monitoring support capacity for fossil CO2 emissions

Project Coordinator: Dr Richard Engelen (ECMWF)
Project Start Date: 01/01/2021
Project Duration: 36 months

Published by the CoCO2 Consortium

Contact:
ECMWF, Shinfield Park, Reading, RG2 9AX,
richard.engelen@ecmwf.int

The CoCO2 project has received funding from the European Union's Horizon 2020 research and innovation programme under grant agreement No 958927.

Table of Contents

Figures

Tables

1 Executive Summary

This deliverable documents the development of the CO_2 regional inverse modelling systems WRF-CTDAS and CIF-CHIMERE in preparation for the use of satellite retrievals from the CO2M mission for estimating CO_2 fluxes from Western European countries. To this end, a pseudo dataset of CO2M satellite retrievals has been made based on an orbit simulator, a CO_2 nature run from the Integrated Forecasting System (IFS) model, and a parameterization of random and systematic retrieval uncertainties. This dataset is used in the WRF-CTDAS inversions to test their ability to recover the fossil and biological CO_2 fluxes that were used in the nature run. The inversion setup is the same as used in the national scale inversions reported in CoCO2 deliverable D4.6. Therefore, we test the ability of the inversions to correct the priors used in that inversion setup to those used in the nature run, which are different and reflect the remaining uncertainties in the spatio-temporal distribution of CO_2 fluxes across the domain. In addition, we investigate the impact of uneven sampling by the CO2M satellite constellation due to cloud cover by redistributing the retrievals randomly across the orbit. Inversions are performed for winter and summer to test seasonal differences in the CO2M inversion performance and the impact of resampling. The results show that resampling has a significant effect. However, the inversion setups have not reached the state yet that robust conclusions can be derived. The deliverables also documents plans for inversions with the CIF-CHIMERE system propagating the retrieval errors from the pseudo CO2M observations, but also of pseudo OCO-2 and surface observations, to quantify the uncertainty in the corresponding emission estimates and demonstrate the added value of the CO2M mission.

2 Introduction

2.1 Background

2.2 Scope of this deliverable

2.2.1 Objectives of this deliverables

The aim of this deliverable is to investigate the representation of satellite data and their uncertainty in inversions. Satellite data are difficult to represent in a statistically consistent manner, not only because the uncertainties of individual satellite retrievals are not statistically independent, but also because the number of available data requires some degree of averaging for which assumptions on the statistics are required. In addition, the data coverage is not even since the sampling is limited to clear sky conditions and the local overpass time of the satellite. This report makes use of global nature runs performed in the Copernicus CO_2 (CoCO2) project (T2.1a) and simulated orbits of the European CO_2 satellite constellation CO2M provided by European Organisation for the Exploitation of Meteorological Satellites (EUMETSAT) to test the capacity of regional scale inverse models to estimate European CO_2 surface fluxes from CO2M satellite data. The focus of this study is on Western European countries.

2.2.2 Work performed in this deliverable

A series of Observing Systems Simulation Experiments (OSSEs) is performed using different inverse modelling systems driven by pseudo data from CO2M (and from OCO-2 and the surface network used in D4.6) focusing on Europe during 2018. The performance of the inversions is measured (1) by their ability to recover the 'true' emissions that were used in the nature run from which the pseudo satellite measurements were sampled, or (2) via the propagation of errors following the error statistics given to the inversion system such as in more traditional inversion OSSEs, including the errors assigned to the satellite or surface observations. The CO2M samples were taken according to simulated footprints of the CO2M

dataset delivered by EUMETSAT. This is done in different ways to investigate the sensitivity of the inversion optimised fluxes to the geographical coverage of the satellite measurements. To make the sampling as realistic as possible, the EUMETSAT dataset has been extended with information on cloud cover. To use the data in the inversion, the random and systematic error components of the satellite retrievals have been estimated as function of their main controlling parameters, including solar and viewing angles, surface albedo, cirrus and aerosol scattering properties, using the equations from Buchwitz et al (2013) adjusted for application to CO2M.

2.2.3 Deviations and counter measures

The execution of the initial plan for T5.4 encountered major difficulties, which forced us to prioritise the most important parts of the work that was planned initially. The first hurdle was a replacement in personnel during the project, linked to the Covid pandemic. In the end we were able to use the PM's allocated to this task, but an important fraction went into the training of newly recruited staff. The second hurdle was a replacement of the Dutch supercomputer with a new machine, which caused unexpected difficulties operating the existing code and using it in computationally demanding production runs. Because of these difficulties the initial plan for CoCO2 Task 5.4 turned out to be too ambitious.
The counter measure was to prioritise on the construction of the CO2M satellite pseudo dataset, which was not foreseen for Task 5.4, but an essential input for the simulations that were proposed and therefore had to be prepared. The delays in the planning had the advantage that output of the CoCO2 nature runs could be used for this. The CO2M pseudo dataset was finally produced late in the project. The inversion development concentrated on the CO2M satellite sacrificing the reference to the use of OCO-2 that was foreseen initially.
The inversions using WRF-CTDAS by VUA were completed, but too little time remained to do this in the iterations needed to solve all intricate issues that are commonly encountered in this process. This prevented us from making the model comparison that was planned in this task, explaining why we focus on results from WRF-CTDAS. On the side of CEA, there was a lack of remaining time to conduct CIF-CHIMERE inversion experiments with this dataset. This deliverable documents the plan that was made for these experiments, and some illustration of the results when assimilating pseudo OCO-2 and surface data. The full inversions planned by DLR were not realised; instead, we demonstrate progress made in WRF-CTDAS model development during CoCO2 with a test case. This deliverable represents the status of regional inversion development for using CO2M data over Europe and its preliminary outcomes, which will continue after the CoCO2 project.

3 Methodology

3.1 Pseudo observations: Carbon Dioxide Monitoring (CO2M) database

For the OSSE experiments conducted in the CoCO2 WP5.4, pseudodata have been created for 2018 for Europe (see section 3.1.1). The pseudo data mimic observations that will be made available by the Copernicus CO_2 satellite mission CO2M. Briefly, the CO2M mission will start in 2025 and will consist of a constellation of three satellites in sun-synchronous orbits (CO2M-A, CO2M-B and CO2M-C). The CO2M satellites will sample along a 250 km wide swath with a pixel size of 4 km^2 (Sierk et al. 2019). The mission will focus on retrieving xCO_2 in the near infrared (NIR) and shortwave infrared spectral range (SWIR) and the NO_2 tropospheric column in the visible spectral range, as well as CH_4 (Sierk et al. 2019; ESA Earth and Mission Science Division, 2020). The satellites will carry a Multi Angle Polarimeter (MAP) and Cloud Imager (CLIM) for measuring aerosols and clouds to minimise the systematic errors in the retrieval methods (Rusli et al, 2021). The satellites overpass a location at 11:30h local time, with a 11-day repeat cycle.

The database includes pseudo data for CO_2, CH_4 and their errors (systematic & random). CO2M orbits and measurement footprints of the CO2I imagers onboard the CO2M satellites were provided by EUMETSAT, based on an orbit simulator considering the orbit parameters and instrument specifications of CO2M. This dataset provides measurement locations, times, footprint coordinates, viewing angles, etc. but no information about greenhouse gas total columns and measurement errors. WP5.4 added that information as described below.

3.1.1 Input data

CO_2 and CH_4 column data (xCO_2 and xCH_4), as well as cloud cover for 2018, are retrieved from a nature run based on a high-resolution version of ECMWF's Integrated Forecasting System (IFS) developed for the Copernicus Atmosphere Monitoring Service (CAMS). More specifically, the CoCO2 nature run v1 uses the latest IFS cycle CY48R1 and anthropogenic emissions from CAMS-GLOB-ANTv5.3 (https://essd.copernicus.org/preprints/ essd-2023-306/, available from the Copernicus Atmosphere Data Store https://ads.atmosphere.copernicus.eu/#!/home). More detailed information about CAMS and IFS can be found in Agustí-Panareda et al. (2022). xCO_2 and xCH_4 pseudo-observations are filtered for clouds using a cloud threshold of 1%, following for example Kuhlmann et al. (2021).
For the CO_2 and CH_4 systematic and random errors we make use of the error parameterization by Buchwitz et al (2013) (see Section 3.1.2), which will be referred to as the B13 method. For this method the following input data are needed: surface albedo at 858 nm and 1640 nm, aerosol optical depth at 550 nm (AOD), cirrus optical depth (COD) and cirrus cloud top height (CTH). For surface albedo monthly climatological fields are used from the Carbon Monitoring Satellite (CarbonSat) database, initially retrieved from MODIS (Technical Note for ESA study; see also here https://www.iup.uni-bremen.de/carbonsat/). Monthly AOD is retrieved from CAMS global atmospheric composition forecasts (v21r1/Innes et al. 2019), while monthly COD and CTH are from the International Satellite Cloud Climatology Project (ISCCP) (Rossow et al. 2016). Due to missing values of COD/CTH ISCCP data over northern America, monthly climatological COD/CTH from the CarbonSat database are used to fill in the gaps. This climatology is based on retrievals from Cloud-Aerosol Lidar with Orthogonal Polarisation (CALIOP)/ Cloud-Aerosol Lidar and Infrared Pathfinder Satellite Observation (CALIPSO) (Technical Note for ESA study). All the input data are for 12:00h UTC.

3.1.2 CO_2, CH_4 systematic and random errors

Systematic and random retrieval errors, SEs and REs from now on, for CO_2 and CH_4 are calculated following B13. The error equations used in this method are a function of AOD at 550 nm, COD, CTH and albedo at 858nm and 1640nm. Further details can be found in Buchwitz et al. (2013) and references therein. Note that REs from B13 are divided by 2.0, to account for an improved signal over noise ratio (SNR) of CO2M compared with CarbonSAT (Wang et al. 2020). It is important to note that flat averaging kernels (AK) were used for xCO_2 and xCH_4, instead of the equations from the B13 method. This simplification was introduced to avoid the complication of reducing the vertical resolution of IFS to the limited number of layers of the satellite retrieval, which should account for differences in the vertical coordinate systems, etc. In the end the impact of this simplification is expected to be small, as the CO2M averaging kernels are approximately uniform in the troposphere.

3.1.3 Retrieval error scaling

To evaluate the CO_2 and CH_4 SE and RE derived from the B13 equations, the data are compared against other simulated CO2M data. More specifically, the CO2M end-to-end simulator Remote sensing of Trace gas and Aerosol (RemoTAP) is used, developed by the Dutch Institute for Space Research (SRON) (Lu et al. 2022). Unlike the B13 method developed for CarbonSat, RemoTAP accounts for the extended capability of CO2M to simultaneously retrieve aerosol and trace gases using the multi-angle polarimeter (MAP) and CO2 imager (CO2I) onboard CO2M. CO2I measures top-of-atmosphere Earth reflected spectral radiance and solar irradiance in three spectral windows; one in the near infrared and two in the short-

wave infrared. MAP measures radiance and degree of linear polarisation at six wavelengths and 43 viewing angles on ground. For more information, please refer to Lu et al. (2022). The regional RemoTAP dataset includes orbits over Europe and America. The original dataset ignores cloud coverage as it focuses on the effect of aerosols on the retrieval for each region. However, to compare with the synthetic CO2M data, RemoTAP data are filtered for cloudy conditions using IFS data and applying the same cloud filtering criteria as for CO2M (see in Section 3.1.1). RemoTAP has the advantage over the B13 method that it was designed to simulate CO2M. However, RemoTap is computationally much more expensive. For this reason, data for only fractions of a few orbits are available. We use these data to scale the errors from the B13 method such that the medians of their statistical distributions agree. This way we account for systematic offsets in the expected instrument performances of CarbonSat and CO2M, although we still rely on the spatial-temporal distribution of uncertainties from the B13 method. They account for dominant influences of surface albedo and viewing angles on the REs, which are valid for CO2M also. However, the spatio-temporal pattern of SE is influenced by the correction of aerosol influences on the light path using MAP data, which our error estimation method cannot account for. Additionally, the use of a dedicated retrieval algorithm for sun glint measurements will improve the CO2M performance over sea (Boesch et al, 2011), which our simplified approach cannot account for.

Figure 3.1.1 shows the distribution of xCO$_2$ REs (RE$_{B13}$/2.0, see Section 3.1.2) and SEs as derived from the B13 method. Unscaled xCO$_2$ SEs and REs range between -1.0 and 1.3 ppm and 0 and 1.2 ppm respectively. Figure 3.1.1 also shows the probability density function of B13 and RemoTAP errors for xCO$_2$. RemoTAP xCO$_2$ errors are expressed as defined 1 sigma uncertainty and therefore only have positive values. Thus, to compare with CO2M xCO$_2$ errors, the square root of the quadratic sum of CO$_2$ REs and SEs is used. As shown in Figure 3.1.1, the majority of CO2M errors lay between 0 and 3 ppm, while the RemoTAP CO$_2$ error ranges between 0 and 3.0 ppm. Note that all three satellites are used for this comparison and all data through 2018. Thus, the scaling factor is estimated as the ratio between the RemoTAP median (1.36 ppm) and Buchwitz median (0.85 ppm). Following the same procedure, the scaling factor for CH$_4$ is also calculated, but the results are not shown in this report.

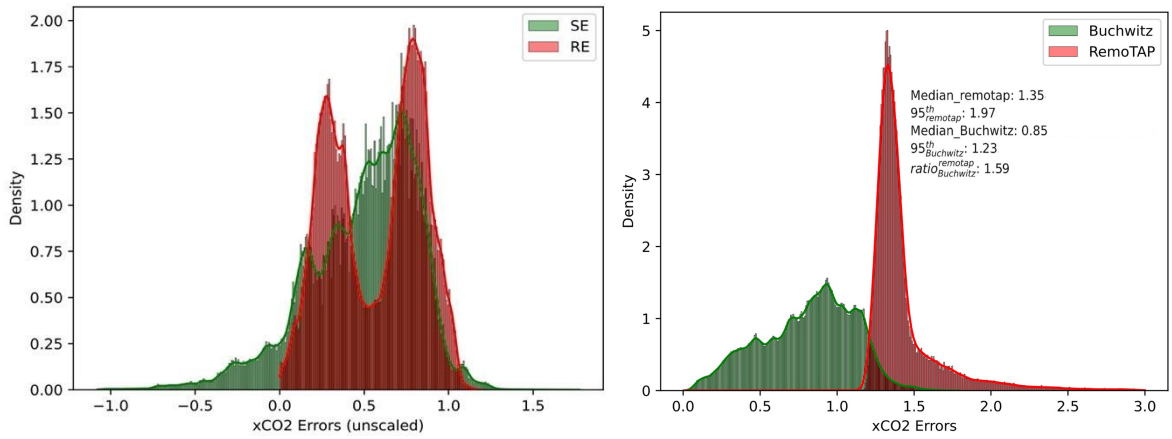

Figure 3.1.1: Distribution of xCO$_2$ REs and SEs errors from the unscaled B13 method (left panel) and a comparison of the quadratic sum of B13 REs and SEs and RemoTAP xCO$_2$ errors. All the errors are in ppm. The lines in both figures show the kernel density function (KDE), while the bars show the errors. Note the different scales.

Figure 3.1.2 shows an example of xCO$_2$ total column, xCO$_2$ REs and SEs for February and in July 2018, using data from all three satellites and after scaling the pseudo data. xCO$_2$ REs

mostly range between 0.01 and 1.2 ppm, with a few higher values in some pixels e.g. over sea in February and from 0.01 to 1.6 ppm in July, also showing some higher errors over sea.

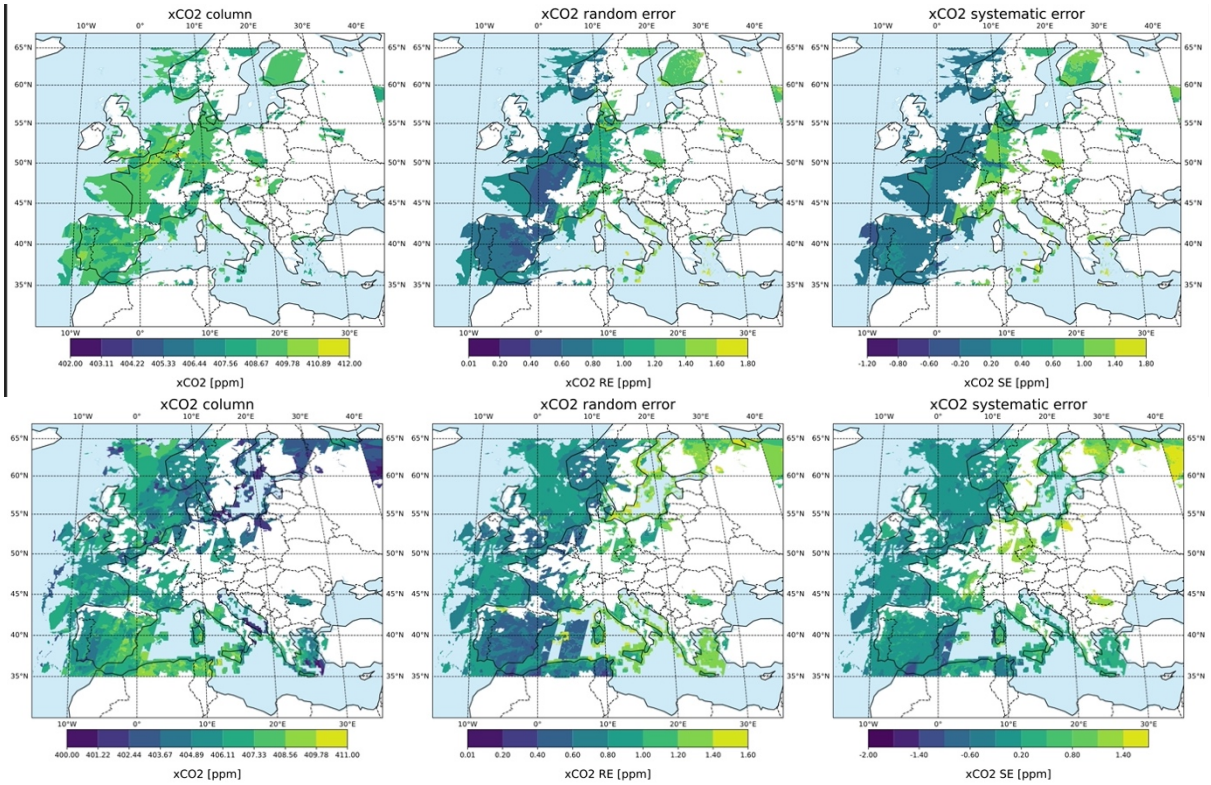

Figure 3.1.2: CO2M orbits for February (upper panel) and July (lower panel) 2018. From left to right: xCO$_2$ column, xCO$_2$ REs and SEs. All in ppm.

xCO2 SEs range between -2.0 and 1.6 ppm in February, while between -2.0 and 1.6 ppm in July. These errors are slightly higher compared to other recent studies, such Kaminski et al. 2022, who used another method (Quantitative Network Design) to estimate the xCO$_2$ errors where the xCO2 RES do not exceed 1.0 ppm and xCO2 SES range between -0.2 and 0.2 ppm for a day (orbit) in February and July.

3.2 Models

Two different models and different inverse modelling configurations are used as part of this deliverable which are described below.

3.2.1 WRF-CTDAS

The CarbonTracker Data Assimilation Shell ("CTDAS", van der Laan-Luijkx et al., 2017), was originally developed for use in combination with the global atmospheric transport model TM5. The inverse modelling framework used here, replaces TM5 with the Weather Research Forecast with chemistry (WRF-Chem) model for regional studies at higher spatial resolution (Grell et al., 2005). WRF-CTDAS was developed and used in the EC funded projects H2020-SCARBO and H2020-CHE (see https://che-project.eu/node/239). Figure 3.2.1 shows the workflow of the WRF-CTDAS system. The Ensemble Kalman Filter (EnKF) method is used in CTDAS to solve the Bayesian optimization problem via pseudo random samples of data providing a statistical representation of the covariance structure in the space of fluxes and mixing ratios (Peters et al., 2005).

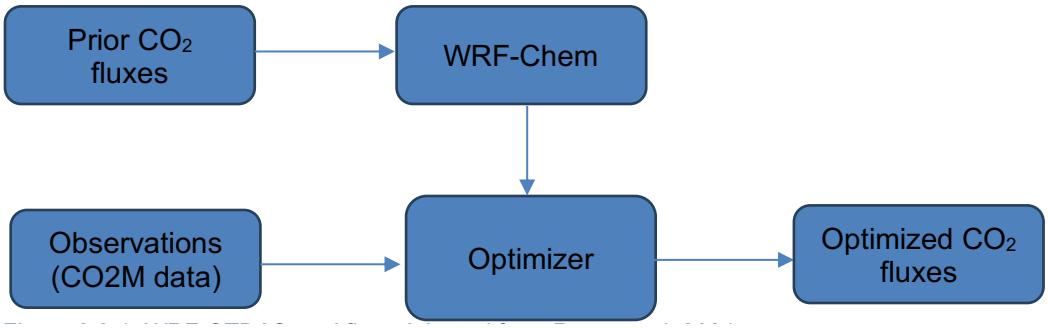

Figure 3.1.3: A schematic representation of the WRF-CTDAS inverse modelling framework.

During CoCO2, we implemented features that allow CTDAS-WRF to optimise fluxes at high spatial resolution: allowing prior flux covariances and replacing the existing localization algorithm with a computationally efficient one based on distance. These features were implemented in collaboration with Tzu-Hsin (David) Ho (MPI-BGC, Jena). Localization is an error prevention method for Ensemble Kalman Filters: since the state vector and its covariances are represented by a finite ensemble, spurious correlations can cause unphysical optimizations and thus degrade the estimated fluxes. The standard localization method in CTDAS is based on a t-test. We found that this approach is computationally not feasible for large state vectors and implemented an alternative localization method based on the distance between the observation and the state vector element location, drastically reducing computational time. We also implemented the ability to assimilate in situ data, which is demonstrated in D4.6.

Table 3.2.1 A summary of the CTDAS configuration by VUA used for the OSSEs.

Table 3.2.1: CTDAS configuration.

Temporal resolution	Assimilation window	Correlation length	State vector resolution	Spatial correlations	Scaling factor
1 week	2 weeks	300km	100km	Yes	Separate for prior fluxes

The temporal resolution in Table 3.2.1 refers to the time resolution at which the surface fluxes in the state-vector are optimised. The assimilation window refers to the width of the time window that the EnKF uses to propagate forward in time. The width limits the timespan of source-receptor relations that are accounted for in the flux optimization. The a priori flux uncertainties are correlated in space as defined by the correlation length. The inversion distinguishes between fossil, biological, and fire fluxes, which are optimised separately.

3.2.1.1 WRF setup

3.2.1.2 VUA

WRF-Chem model version 4.1.1 (Skamarock et al. 2019) is used in this study. The greenhouse gases (GHG) module is used to calculate CO_2 transport (Grell et al.2005; Beck et al., 2011). All other atmospheric chemistry options are switched OFF as they are not needed for the long-lived trace gas CO_2, while state of the art schemes are used for simulating atmospheric transport.
The model is run over Europe using two domains (see Fig. 3.2.2), where the parent domain (d01) covers the whole of Europe, and the nested domain (d02) covering Western Europe. The boundary and initial conditions are derived from the IFS nature run (see above in Section 3.1.1**)** for CO_2 and from ECMWF Reanalysis v5 (ERA5) for meteorological parameters (Hersbach et al., 2023 a, b). 100 ensemble members are used and a total of 50 vertical levels and spectral nudging for d01 and d02 are used. WRF-Chem temperature, wind and humidity are nudged at each dynamical step toward the reanalysis and are updated every 3h above the atmospheric boundary layer. Different simulations are performed in this study, summarised in Section 3.3.

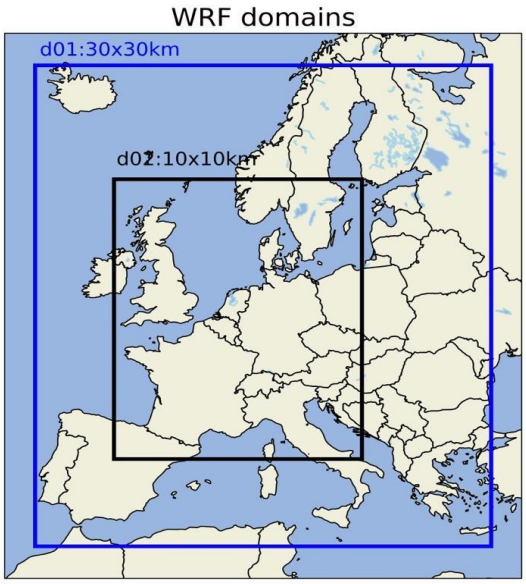

Figure 3.2.2: WRF domains at 30km (d01) and 10km (d02).

3.2.1.3 DLR (test case)

Here, we use the transport model WRF-GHG version 4.3.3. The domain of the test case covers portions of southern Europe in 12x15 grid cells with a resolution of 100 km, 39 vertical levels and a time step of 10 minutes (see e.g. Fig. 3.4.2.1). This configuration is designed to allow fast runs of the transport model instead of optimising accuracy. The model is driven by meteorological fields from ERA5 (Hersbach et al. 2017, 2023a). Atmospheric transport is computed for an ensemble of 150 passive tracers.

3.2.2 CIF-CHIMERE (for France)

The CIF-CHIMERE inversion configuration for France developed in the framework of task T4.4 (WP4) of the CoCO2 project should have been used to conduct OSSEs with the assimilation of the pseudo CO2M data produced in this task, in addition to pseudo OCO-2 and surface CO_2 data corresponding to the real data assimilated in the CIF-CHIMERE inversions in T4.4 (see D4.6 of WP4). These OSSEs correspond to the inversion of the national scale estimate of hourly CO_2 flux maps in France over a full month (July 2018). In these OSSEs, the concept was to compare the skill for monitoring the CO_2 anthropogenic and natural fluxes when assimilating CO2M data vs. when assimilating data from the current observation networks, depending on the CO2M sampling, and to assess the relative weight of the random and systematic errors in the CO2M data on the uncertainty in the fluxes from the inversions. For this purpose, these OSSEs propagate the errors corresponding to these datasets, in addition to the uncertainties from the prior estimate of the fluxes and to the transport modelling errors, assuming that the statistics for all these errors are perfectly characterised in the inversion set-up. First tests of OSSEs assimilating pseudo OCO-2 and surface data were conducted, but the pseudo CO2M data were not made available early enough to finalise the overall ensemble of OSSEs. In particular, this ensemble does not include the tests with CO2M.

General information about the CIF CHIMERE variational inversion system for France

The CIF-CHIMERE system used here relies on the coupling between the variational mode of the CIF (Berchet et al., 2021), the regional chemistry transport model CHIMERE (Menut et al., 2013) and the adjoint of this model (Fortems-Cheiney et al., 2021).

CHIMERE configuration for France

The configuration of CHIMERE (and of its adjoint code) for France covers the domain: 11°W-12°E ; 39,5°N-54,5°N (cf Figure 3.2.2.1). Its zoomed grid has a 10 km horizontal resolution over France, and a 50 km horizontal resolution in the corners of this domain (Figure 3.2.2.1). It has 20 vertical layers, from the surface to 200hPa. The modelling of the CO_2 concentrations above 200hPa for comparisons to CO_2 total column concentrations (XCO_2) from satellite instruments relies on the product used to impose the model initial and boundary conditions. CHIMERE is driven by the ECMWF / IFS operational meteorological forecasts.

Control vector

The CIF-CHIMERE inversions of the CO_2 fluxes in France over July 2018 control separately the anthropogenic, terrestrial ecosystem and ocean CO_2 fluxes in addition to the model initial and boundary conditions for this month. In particular:

- the anthropogenic (fossil fuel and biofuel) emissions are controlled at the scale of 5 aggregated sectors of activity (public power, industry, other stationary combustion, road transport, other) per administrative region (in France) and per country (outside of France), and at 1-day temporal resolution
- the ocean and terrestrial ecosystem fluxes are controlled at the model grid-cell (i.e. 10 km over France) and 6-hourly resolution

Other inversion parameters

In the frame of T4.4 in WP4, various experiments have been conducted with this CIF-CHIMERE configuration using different products for the prior estimates of the control vector, assimilating different datasets of real and pseudo-observations, and varying some of the system parameters. A description of the CIF-CHIMERE configuration parameters, of these datasets and of the results are provided in deliverable D4.6. Here, a specific set-up of the CIF-CHIMERE configuration is used to conduct the OSSEs with the inversion of the CO_2 fluxes in France in July 2018 as detailed below and in sections 3.3 and 3.4.

For both the in situ and satellite observations the inversion systems accounts for both transport model and observation errors. The observation error covariance matrix of the system is set-up as a diagonal matrix (without spatial or temporal correlation across the observations) with the observation error values provided in the observation products, and with values for the transport model error for the in situ and satellite observations respectively taken from Broquet et al. (2013) and Potier et al. (2022).

The set-up of the part corresponding to the CO_2 natural fluxes in the prior uncertainty covariance matrix in the system is derived from that of the PYVAR-CHIMERE CO_2 NEE inversions in Monteil et al. (2020), albeit with 100-km scale spatial correlations for the terrestrial ecosystems (instead of 200-km spatial correlations, since the system operates at much higher spatial resolution here) and some other slight differences. The set-up of the part corresponding to the CO_2 anthropogenic emissions in the prior uncertainty covariance matrix assumes a 50% 1-sigma uncertainty in the total emissions per administrative region and day (i.e. a bit more than 100% 1-sigma uncertainty in the total emissions per large sector of activity, administrative region and day). It ignores spatial correlations across the regions, and temporal day-to-day correlations. The prior uncertainty in the boundary conditions is characterised by a 500 km horizontal correlation scale and by a 2 ppm 1-sigma uncertainty in the total columns in the prior error covariance matrix. The prior uncertainty covariance matrix does not include any correlation between the different main components of the control vector (ocean, terrestrial ecosystem and anthropogenic fluxes, and boundary conditions).

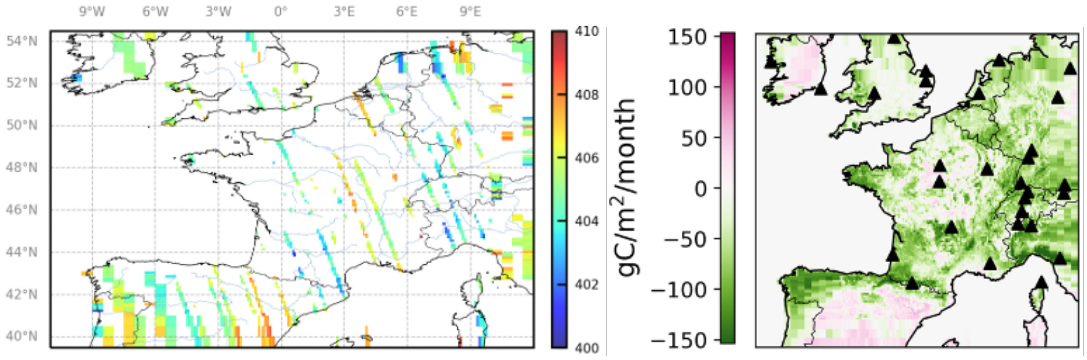

Figure 3.2.2.1: domain of the CIF-CHIMERE inversions and illustrations of its zoomed grid from experiments in Task T4.4 in CoCO2 WP4: 1) (left): binning into the CHIMERE zoomed grid of the satellite OCO-2 v11 observations during the month of July 2018 2) (right): ground based CO2 measurement stations used for the inversions and prior estimate of the CO2 NEE from VPRM interpolated on the CHIMERE zoomed grid during the month of July 2018.

3.3 Simulations

3.3.1 VUA

WRF-CTDAS is run from 15 January to the end of February and 15 of June to the end of July 2018. The first 15 days in each period are considered as spin up and therefore excluded from the analysis, which focuses on one month per run (February and July 2018). The BASE simulation and the different sensitivity runs are described in Table 3.3.1. The results are discussed in Section 4. The TEST and BASE simulations are the same except that the base simulation resamples each CO2M orbit randomly, conserving the number of valid retrievals per orbit.

Table 3.3.1: WRF-CTDAS inversions.

Simulations	Description
BASE	CO2M retrievals only for cloud free scenes
TEST	CO2M retrievals are randomly sampled over each orbit

3.3.2 DLR (test case)

To demonstrate the new capabilities that we integrated into WRF-CTDAS within CoCO2, we ran one test case for 2 days, 1-2 June 2015.

The state vector consists of scaling factors for the three prior flux components at the same extent and resolution as the transport simulation grid, i.e. 12x15 grid cells at 100 km resolution. In addition, one boundary condition offset per corner is optimised, for a total of 544 state vector elements (3*12*15 + 4=544).

Prior uncertainties are 30% for anthropogenic emissions, 50% for GPP and respiration and 5 ppm for boundary conditions. Prior correlations of flux scaling factors are Gaussian with 400 km correlation length and 0.25 for the boundary condition offsets. The temporal resolution is 1 day with an assimilation window of 2 days.

Synthetic observations are evenly distributed over the grid (Fig. 3.2.2.1). The same locations, time of day and values are used for both days.

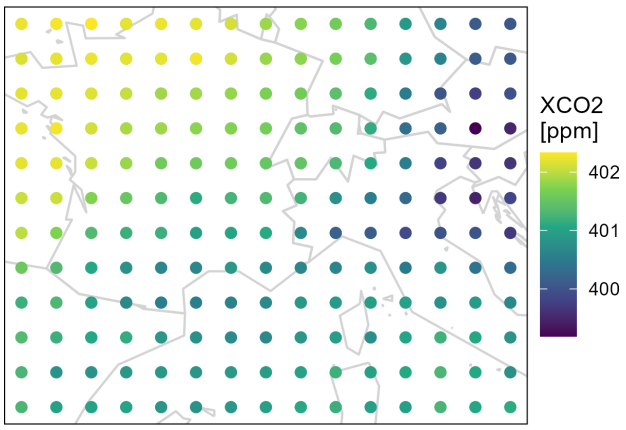

Figure 3.2.2.1: Synthetic observations assimilated in the test case by DLR.

3.3.3 LSCE

The CIF-CHIMERE OSSEs follow the framework of twin experiments. The concept is to assume that the fluxes and simulations of concentrations using the reference products in input of CHIMERE (see section 3.4.3) correspond to the truth, and to perturb them according to the statistics of prior and observation (and model) uncertainties to define the prior estimate and the observations of the inversion. More specifically, for CO2M, the system would have assimilated a simulation of the CO2M XCO$_2$ dataset, using the true CO$_2$ field, the vertical sensitivity and spatial and temporal sampling of the CO2M observation dataset and perturbations corresponding to the statistics of the observation errors (with or without random and systematic errors) as detailed in section 3.1; all individual OCO-2 and CO2M observations are (would have been) simulated and assimilated using the grid-cell of CHIMERE containing the centre of their corresponding CO2M pixel (there is no aggregation of the satellite observations at the model resolution)

By doing so, one propagates the prior and observation errors into the system to derive an estimate of the posterior uncertainties in the estimates of the fluxes from the inversion. The comparison between posterior and prior error to the truth would have provided a direct assessment of the potential of the OCO-2, surface, and CO2M observations depending, for the latter, on the corresponding observation errors and sampling configuration.
In practice, the only tests of CIF-CHIMERE OSSEs that have finally been conducted for this deliverable (for the month of July 2018) have assimilated pseudo in situ hourly CO_2 observations from ground based continuous measurement stations in France and in its vicinity (mainly from the ICOS network, all actual data behind the simulation of the pseudo data here being accessed from the ICOS carbon portal, https://data.icos-cp.eu/portal/), and pseudo XCO_2 observations from the OCO-2 NASA-JPL mission (corresponding to the v11 dataset, cf Figure 3.2.2.1).

3.4 Prior fluxes

3.4.1 VUA

Table 3.4.1 summarises the prior CO_2 fluxes and corresponding uncertainties that were used in the VUA inversion setup.

Table 3.4.1: Prior CO_2 fluxes.

Prior Fluxes	Resolution	Prior Uncertainties	Courtesy
Anthropogenic	6x6km	30%	TNO, Hugo Denier van der Gon
Biogenic (respiration & gross primary productivity)	1x1km	50%	VPRM, Julia Marshall
Fire	0.1x0.1	50%	GFAS, Julia Marshall
Oceanic	0.25x0.25	not optimised	Cyril Germineaud, Mercator
Lateral	8x8km	not optimised	LSCE (CEA/CNRS/UVSQ) - IPSL

For anthropogenic CO_2 emissions we use the TNO anthropogenic emission inventory at 6x6 km^2 resolution, which covers the whole of Europe. Lateral fluxes account for the transport of crops and wood, and displacement of CO_2 emissions from production regions. Similarly, the displacement of CO_2 sources and sinks from carbon transport in rivers, lakes, and reservoirs is accounted for. The uncertainties on prior fluxes are chosen following recent papers (Reum et al, 2021, Monteil et al., 2020). An example of anthropogenic and biogenic CO_2 fluxes for a single day in February and July 2018 is shown in Figure 3.4.1 for WRF domain d01. All CO_2 fluxes are used in the simulations, while only anthropogenic, biogenic and fire fluxes are optimised. As a result, 6224 flux parameters are optimised. Also 8 boundary condition parameters are optimised, with a sigma equal to 6 ppm for boundary condition optimisation. Finally, the correlation for neighbouring boundary condition parameters is set to 0.25.
Fossil and biogenic CO_2 prior and posterior fluxes are compared to the “true" fluxes used in the IFS simulations (see in Section 4.1.1). For the IFS simulations CAMS global anthropogenic emissions version 7.0 are used (see Section 3.1.1 for more information), while the net ecosystem exchange biogenic fluxes are generated as part of the IFS simulation and are available for 2021. For fire emissions GFAS are also used for the IFS simulations, so truth and prior fire emissions are the same.

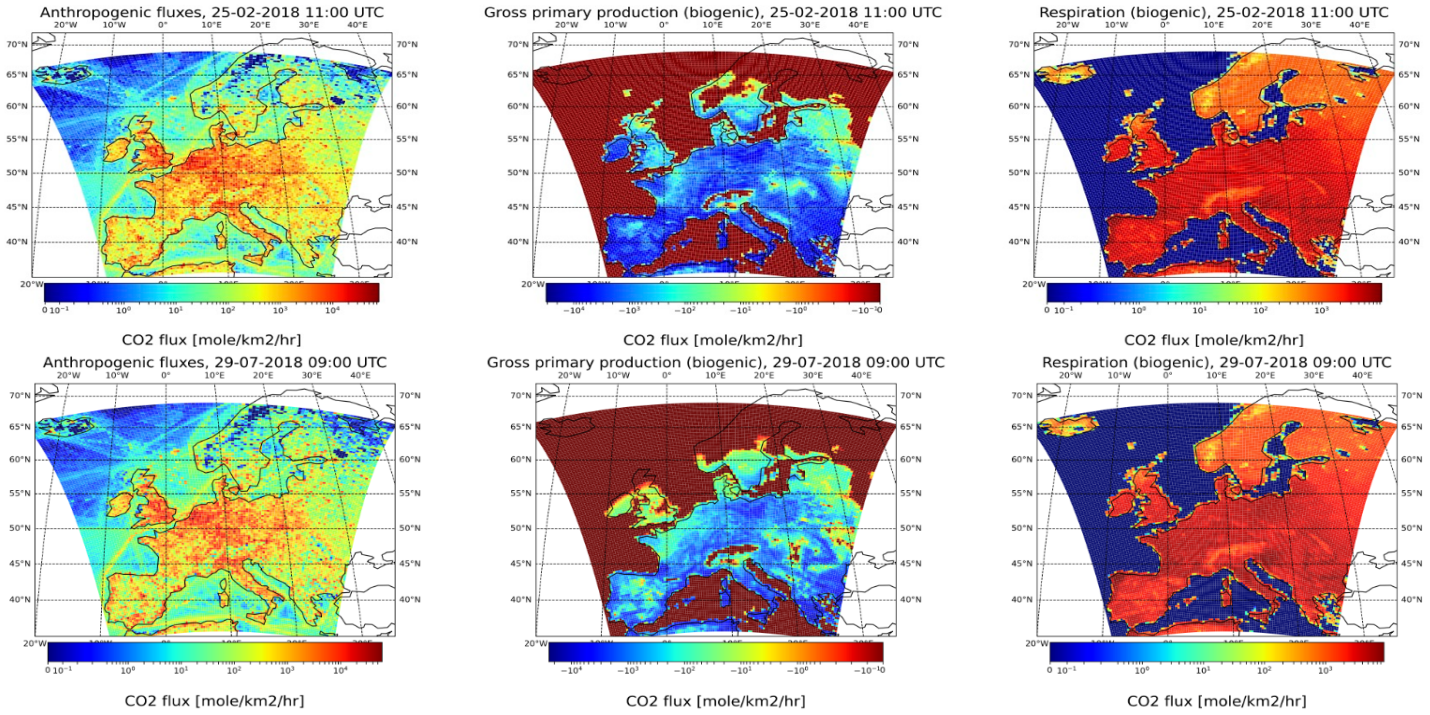

Figure 3.4.1: From left to right figure: anthropogenic and biogenic prior CO_2 fluxes, in mole/Km^2/hr, interpolated to WRF d01 domain. Upper panel shows prior CO_2 fluxes for 25 February 2018 at 11 UTC. Lower panel shows prior CO_2 fluxes for 29 July 2018 at 09 UTC. Note the logarithmic scale.

3.4.2 DLR (test case)

In the test case, we optimise CO_2 emissions. Prior fluxes are composed of 3 datasets: anthropogenic emissions, gross primary production (GPP) and respiration. Anthropogenic emissions are taken from the TNO GHGco dataset (Super et al., 2020), with a resolution of 1/60 x 1/120°. GPP and respiration are from a run of the model VPRM, originally produced in the H2020 project CHE (https://www.che-project.eu/node/149), with a resolution of 5 km. These datasets have then been projected onto the WRF domain (Figure 3.4.2.1).

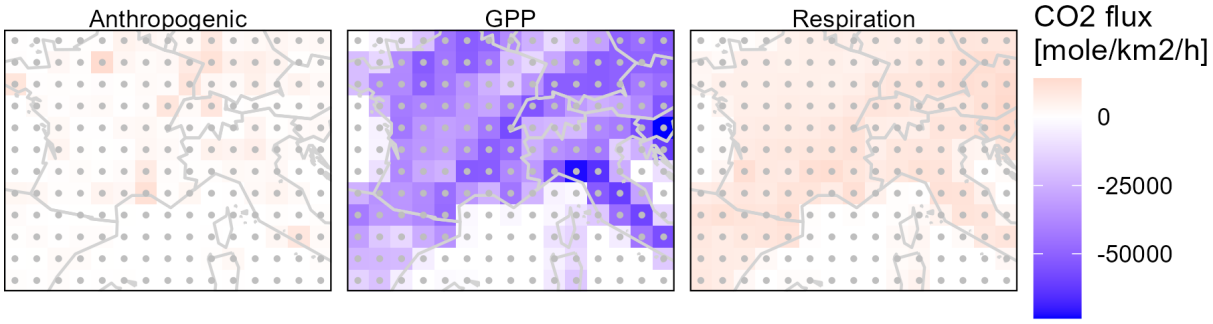

Figure 3.4.2.1: Prior CO_2 emissions for the WRF-CTDAS test case and the synthetic locations of assimilated data as grey dots (one observation per grid cell). Shown here are values for 2015-06-01 12 UTC.

3.4.3 LSCE

Table 3.4.3.1 summarises the products used in CIF-CHIMERE inversions as true estimates of the fluxes when propagating the pseudo-observation errors in the twin experiments.

These true fluxes consist in the anthropogenic emissions and terrestrial ecosystem fluxes from the TNO inventory and Vegetation Photosynthesis Respiration Model (VPRM) simulations delivered in the frame of WP2 (Denier van Der Gon et al., 2022), listed as standard products in the Task T4.4 modelling protocol (see CoCO2 deliverable D4.6). The true initial and boundary conditions are derived from the CAMS global CO_2 inversions v20r2 (assimilating surface data). The true sea/ocean fluxes within the CHIMERE domain are based on a hybrid product from the H2020 VERIFY project at 0.125° resolution combining the University of Bergen coastal ocean flux estimates from the University of Bergen and a global ocean estimate from MPI-BGC-Jena (McGrath et al., 2023). Other types of fluxes are ignored in the CIF-CHIMERE inversion set-up for the OSSEs. The corresponding simulations with CHIMERE are used to represent the true concentrations.

The inversions are conducted with prior estimates of the control variables derived from perturbations of the "true" control variables corresponding to the assumed statistics of the prior uncertainty detailed in 3.2.2, and assimilating observations derived from perturbations of the "true" observation vectors (the true XCO_2 or CO_2 pseudo-observations) corresponding to the assumed statistics of the observation errors.
The potential of the inversions is assessed in terms of misfits between the retrieved fluxes and the "true" fluxes.

Table 3.4.3.1: True CO_2 fluxes for the CIF-CHIMERE inversion OSSEs.

Prior Fluxes	Resolution	Prior Uncertainties	Source, Courtesy
Anthropogenic	6x6km	50% at the scale of 1-day and 1 administrative region in France	TNO TNO_GHGco_6x6km_v4_0_year2018 inventory from CoCO2 WP2, Hugo Denier van der Gon
Biogenic (respiration & gross primary productivity)	1x1km	Configuration derived from that of the PYVAR-CHIMERE CO_2 NEE inversions in Monteil et al. (2020) with a 100-km spatial and 30-day temporal correlation length scale	VPRM simulations from CoCO2 WP2, Julia Marshall
Fire	NA	NA	None
Oceanic	0.125°x0.125°	Configuration derived from that of the PYVAR-CHIMERE CO_2 NEE inversions in Monteil et al. (2020) with a	Hybrid product from H2020 VERIFY, University of Bergen / MPI-BGC-Jena

		1000-km spatial and 30-day temporal correlation length scale	
Lateral	NA	NA	None

4 Results

The sections below show the results from the WRF-CTDAS inversion systems and for the different experiments (BASE, TEST) performed. The results are for February and for the first week of July 2018. It also illustrates the preliminary tests of OSSEs with CIF-CHIMERE when assimilating pseudo OCO-2 and surface data.

4.1 VUA

4.1.1 CO_2 OSSEs using CO2M pseudodata

In this section the OSSEs using unperturbed CO2M pseudodata are presented (BASE simulation). First the results for anthropogenic and biogenic CO_2 fluxes are shown, followed by the results for all optimised fluxes (anthropogenic, biogenic and fire). Fire CO_2 fluxes are negligible over Europe during winter. Figure 4.1.1 shows the true, prior, posterior anthropogenic CO_2 fluxes as well as their differences, over wider Europe (d01).
The posterior CO_2 anthropogenic fluxes are increased over several big cities, such as London, Paris, Hamburg, and Rome. This increase degrades the correspondence with the truth. The reason must be compensation for corrections in the biospheric fluxes. The anthropogenic emission changes smoothen the a priori flux distribution map (for example over Belgium), which is expected from the dispersion of emissions in the atmosphere in a transport model with a limited horizontal resolution compared with the size of cities. Note that the inversion setup is meant for regional scale inverse modelling and can therefore not be expected to properly resolve the scale of cities (for which another inversion setup would be needed).

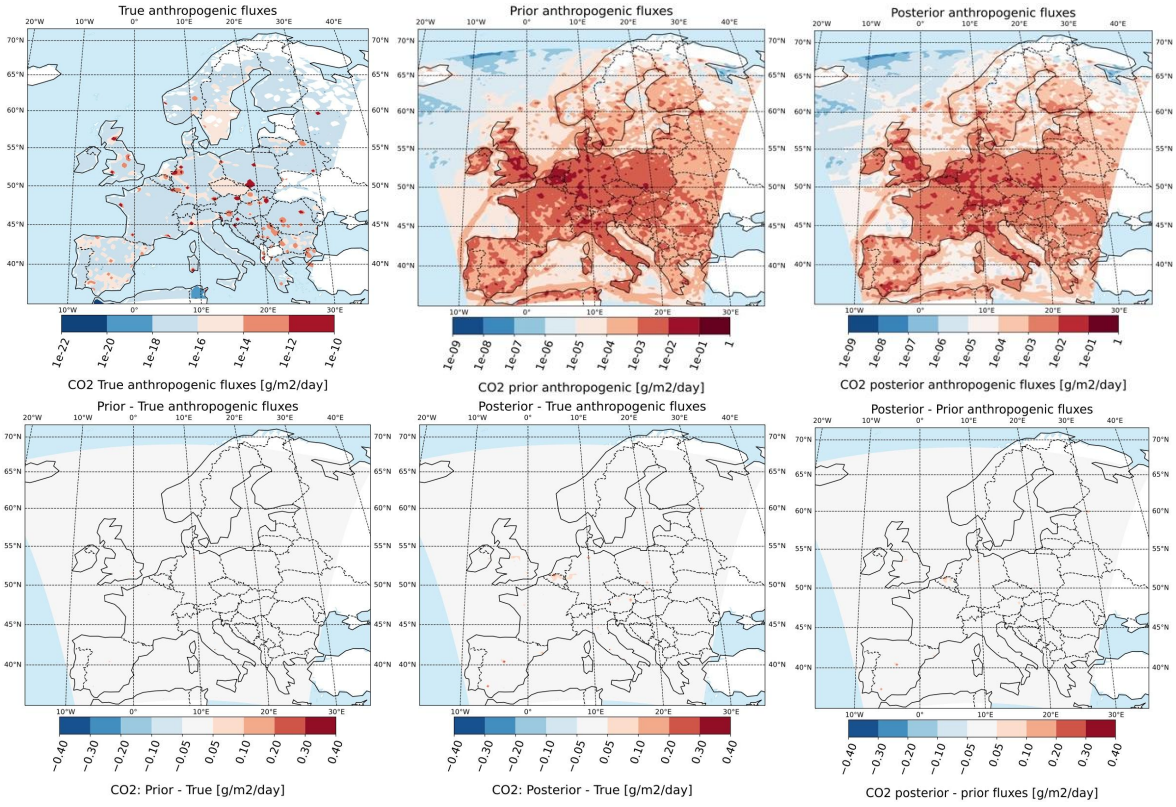

*Figure 4.1.1: Average CO_2 anthropogenic fluxes for February 2018, over wider Europe (d01) and in g/m^2/day. From left to right: **Upper panel shows** true, prior, and posterior fluxes. **Lower panel** shows prior minus true, posterior minus true and posterior minus prior.*

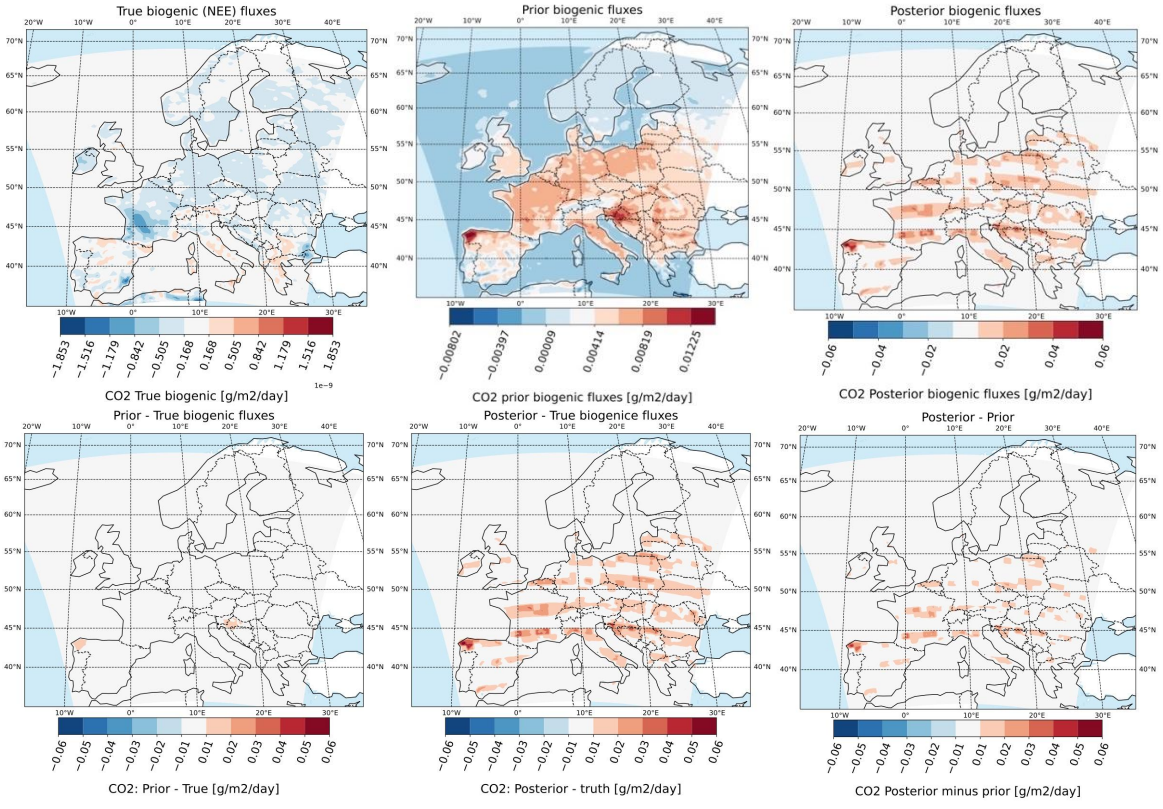

Figure 4.1.2: The same as Figure 4.1.1, but for biogenic CO_2 fluxes.

The “stripe” patterns shown in Figure 4.1.2, for example in the differences between posterior and prior biogenic fluxes, is due to an error that was found in the spatial localization code, causing regions close to the observations not to become optimised (for details see Section 4.1.2). Insufficient time remained to solve the problem for this deliverable report, unfortunately, which would require relaunching all simulations.

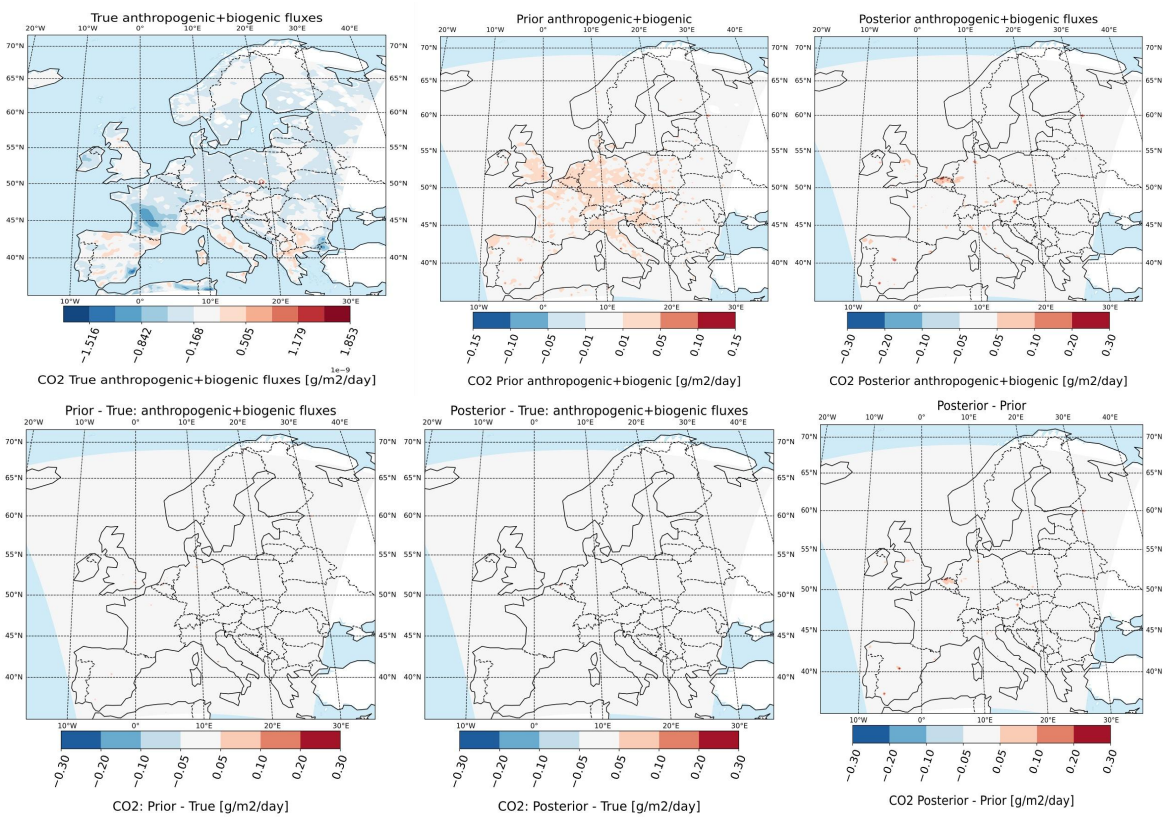

Figure 4.1.3: The same as Figure 4.1.1, but it shows the average sum of anthropogenic and biogenic CO$_2$ fluxes compared to the sum of true fluxes.

Finally, Figure 4.1.4 shows the average prior and posterior anthropogenic and biogenic CO$_2$ fluxes for different countries over Europe. Anthropogenic CO$_2$ seems to be up to two times higher in Belgium and Netherlands compared to the prior information, where CO$_2$ ranges between 35 and 55 Mt CO$_2$/year.

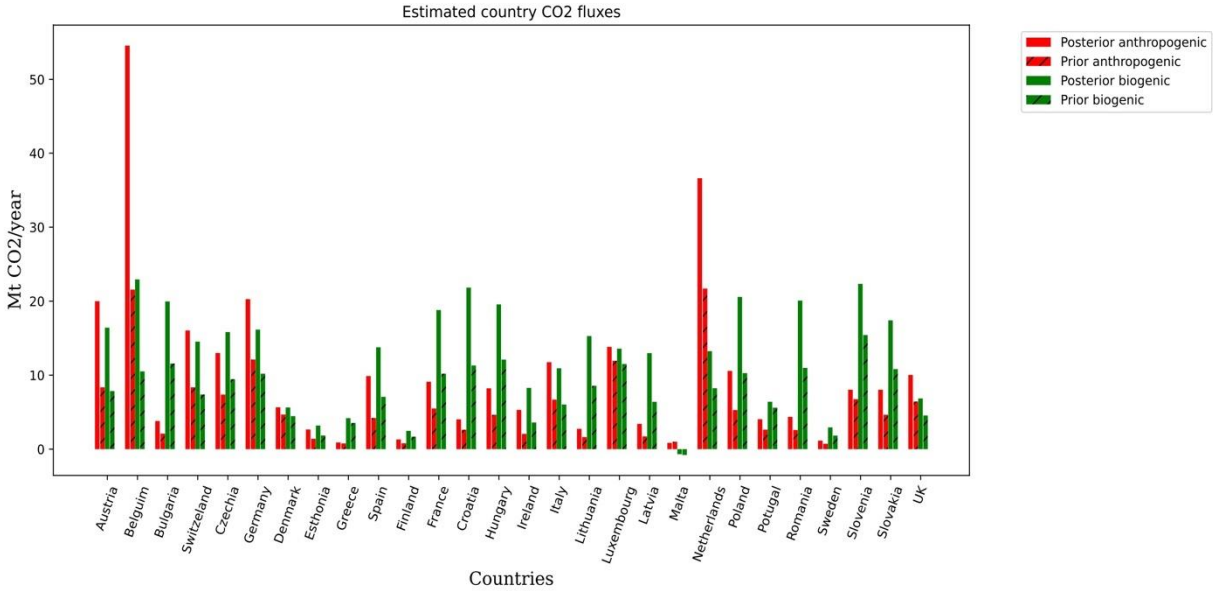

Figure 4.1.4: Averaged prior and posterior anthropogenic (in red) and biogenic CO_2 fluxes (in green) for February 2018 and for the different countries included in the simulation domain (d01).

The figures below (Figure 4.1.5 to 4.1.7) show first results for 1 week of simulation for July (1 to 7) 2018, where more satellite data are available due to less clouds.

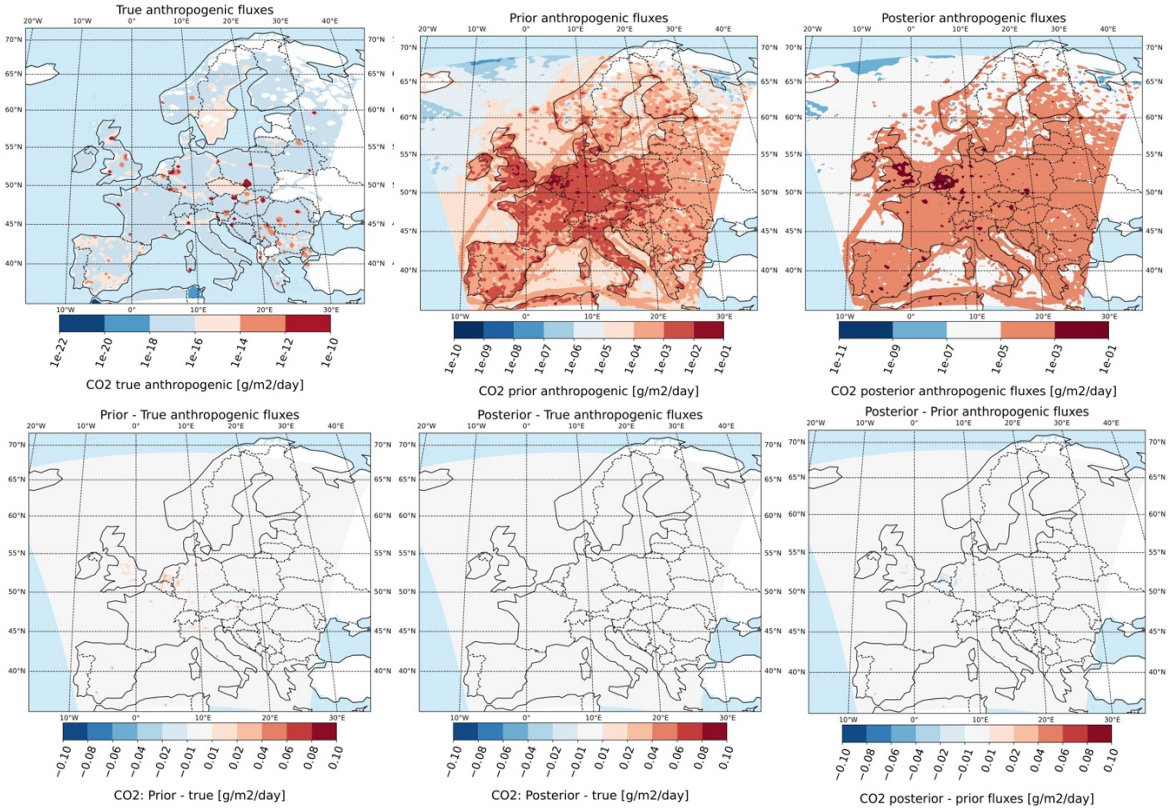

Figure 4.1.5: As Figure 4.1.1, but for the first week of July 2018.

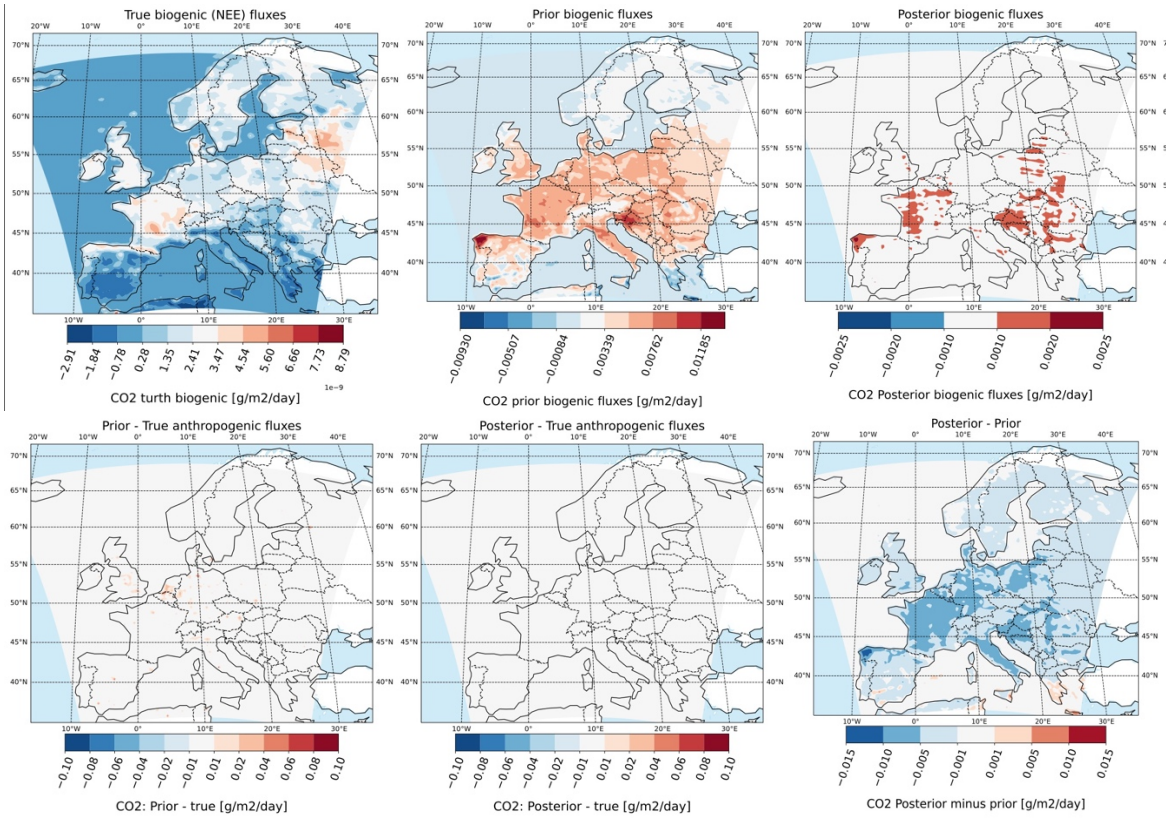

Figure 4.1.6: The same as Figure 4.1.2, but for the first week of July 2018.

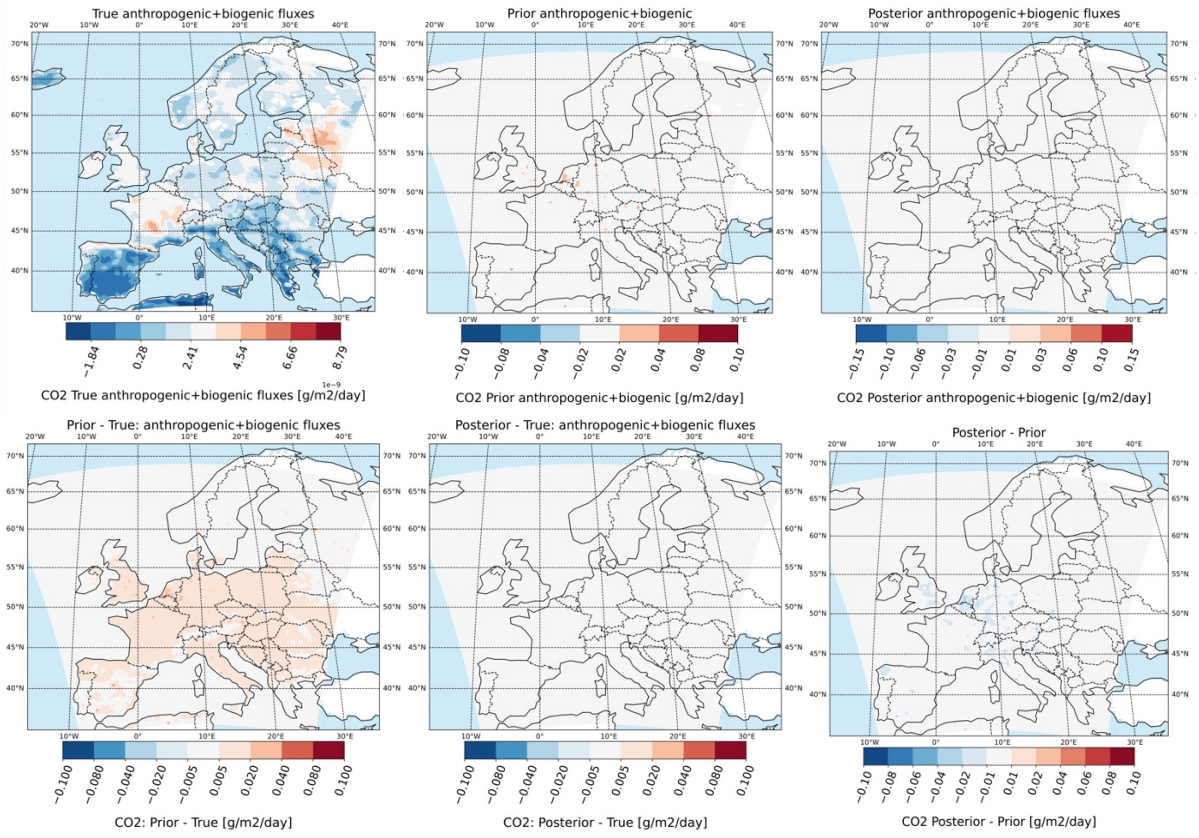

Figure 4.1.7: The same as 4.1.3, but for the first week of July 2018.

4.1.1.1 CO_2 OSSEs using CO2M pseudodata randomly distributed

To evaluate the performance of the OSSEs simulation using the CO2M data described in the previous section, another simulation is carried out using CO2M data, however now the data are randomly distributed over the domain (simulation TEST, Table 3.3.1). The same amount of data is used as in the BASE version.
Figure 4.1.1.1 shows an example of a few CO2M orbits for February and July 2018 where the data are randomly distributed.

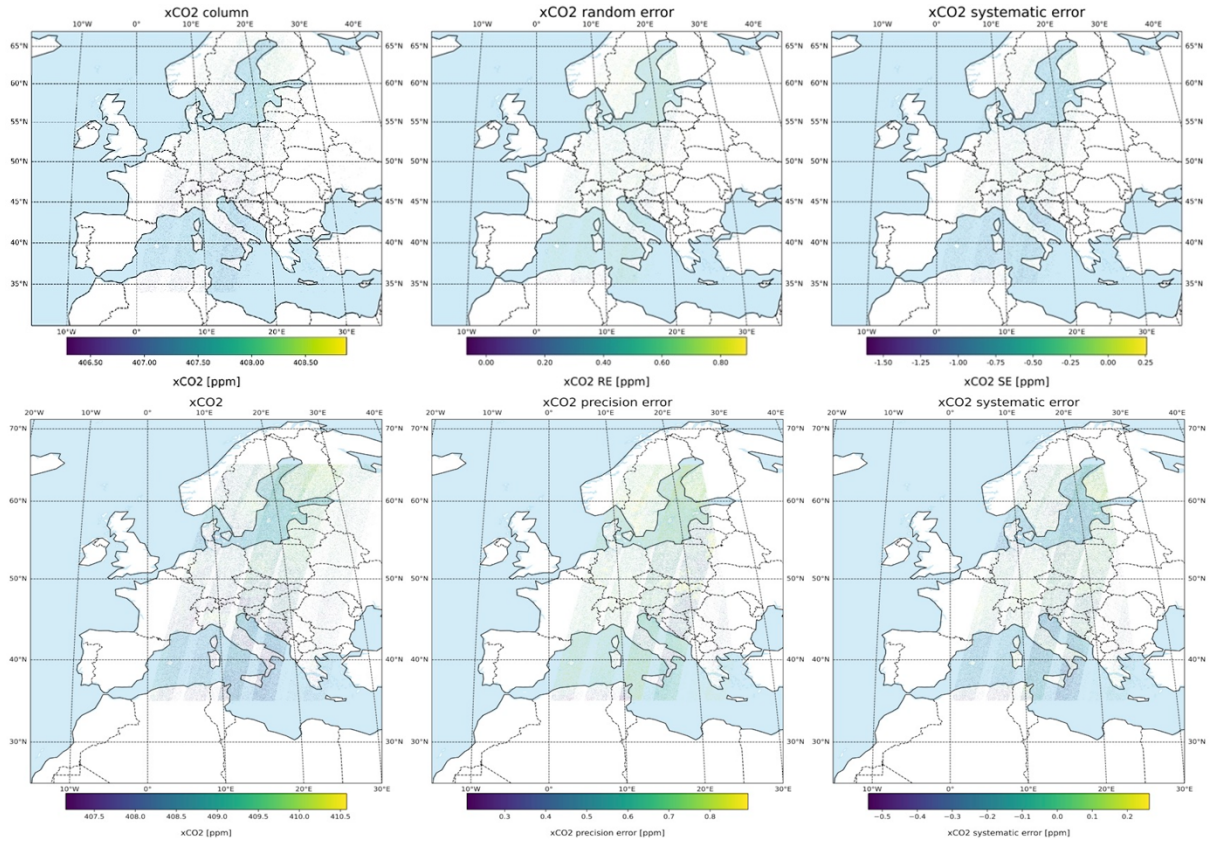

Figure 4.1.1.1: The same as Figure 3.1.2, but CO2M orbits randomly distributed.

Here (Figure 4.1.1.2) only the differences between posterior and truth and posterior and prior are shown, as the truth and prior CO_2 fluxes are the same as in the previous section (Section 4.1.1.1).

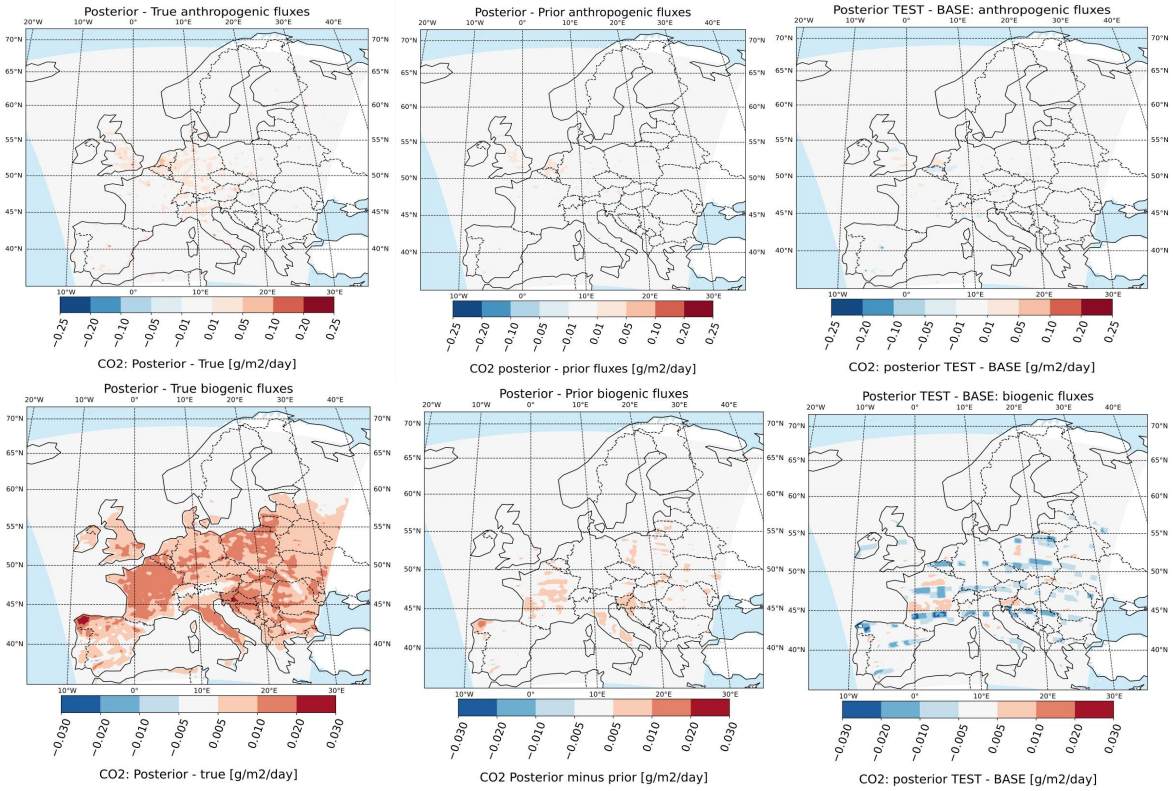

Figure 4.1.1.2: From left to right: Average differences of CO_2 fluxes between posterior and true, posterior, and prior and posterior-TEST and posterior-BASE simulation for February 2018. Upper part shows the results for anthropogenic fluxes, while the lower part shows the results for the biogenic fluxes.

By using randomly distributed CO2M pseudodata (not accounting for cloud cover regions) the posterior CO_2 anthropogenic fluxes are slightly closer to the truth fluxes compared to the results shown in the previous section.

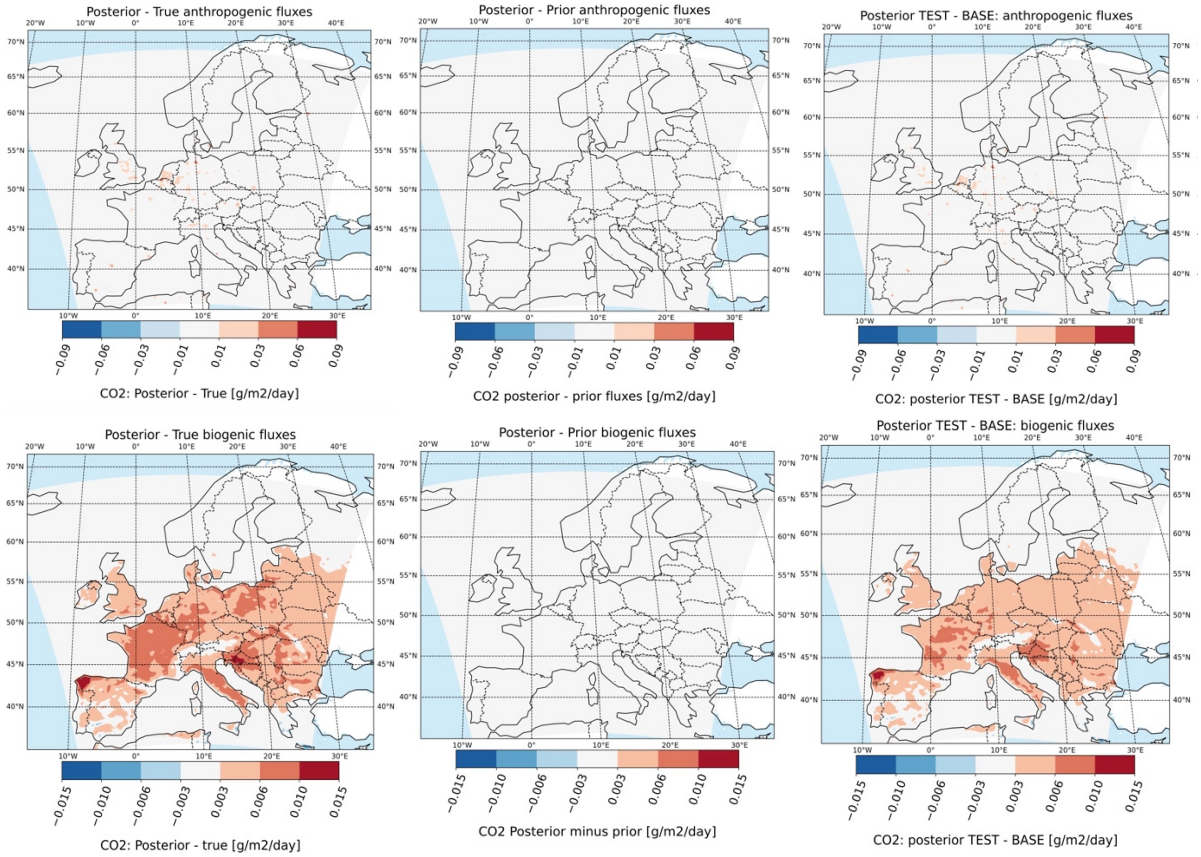

Figure 4.1.1.3: The same as Figure 4.1.1.2, but for the first week of July 2018.

4.1.2 DLR (test case)

Figure 4.1.2.1 shows the inversion increments, i.e. the difference between posterior and prior flux. The differences to the prior fluxes are small (cf. Figure 3.4.2.1), which is not surprising given the low reductions of prior uncertainty (Figure 4.1.2.2). These results are due to the low number of assimilated synthetic observations (180 per day).

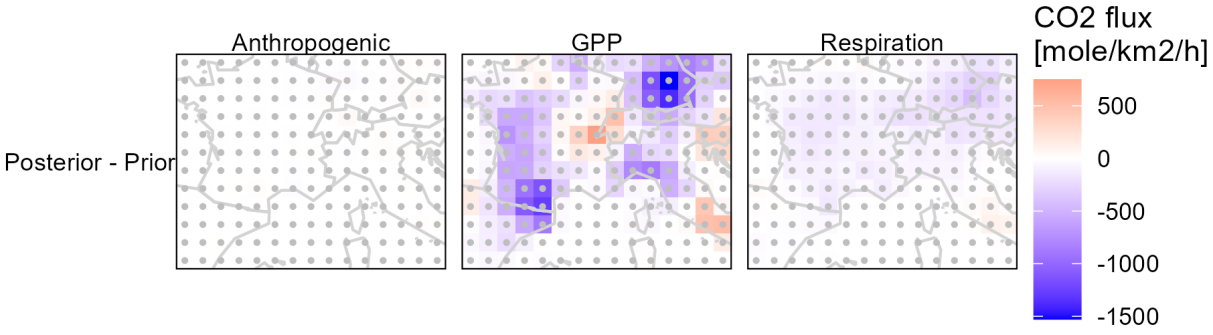

Figure 4.1.2.1: Difference between prior and posterior CO_2 emissions for the WRF-CTDAS test case and the synthetic locations of assimilated data as grey dots (one observation per grid cell). Shown here are values for 2015-06-01 12 UTC.

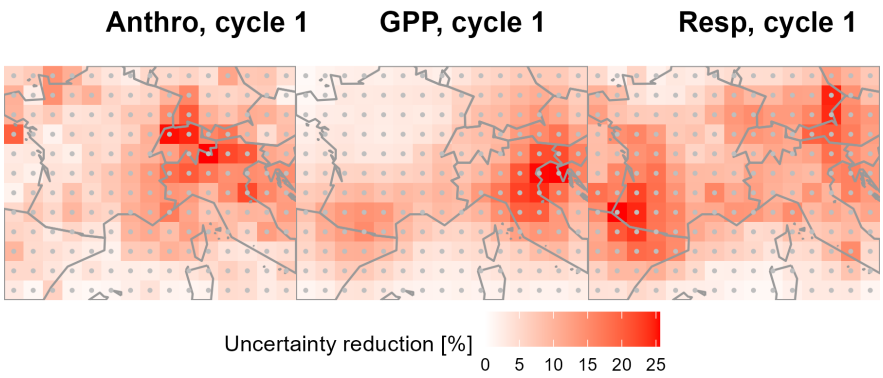

Figure 4.1.2.2: Reduction of random uncertainty for 2015-06-01.

At a late stage of the project, we discovered a bug in the newly implemented spatial localisation code. The bug led to an incorrect mapping of localisation coefficients, which erroneously suppressed some state vector optimizations and erroneously allowed others, potentially spurious ones (i.e. far from the stations). In Figure 4.1.2.1 and 4.1.2.2, the bug has been corrected. However, it was too late to rerun the inversions by VUA (Section 4.1). To illustrate the effect of the bug, below are plots of the test case while the bug was still present (Figure 4.1.2.3 and Figure 4.1.2.4). The large-scale structure of the inversion increments is similar to the ones of the debugged fluxes, but there is an erroneous stripe pattern (cf. Figure 4.1.2.1 vs Figure 4.1.2.3) owing to the bug in the mapping in the localisation code (cf. Figure 4.1.2.2 vs Figure 4.1.2.4).

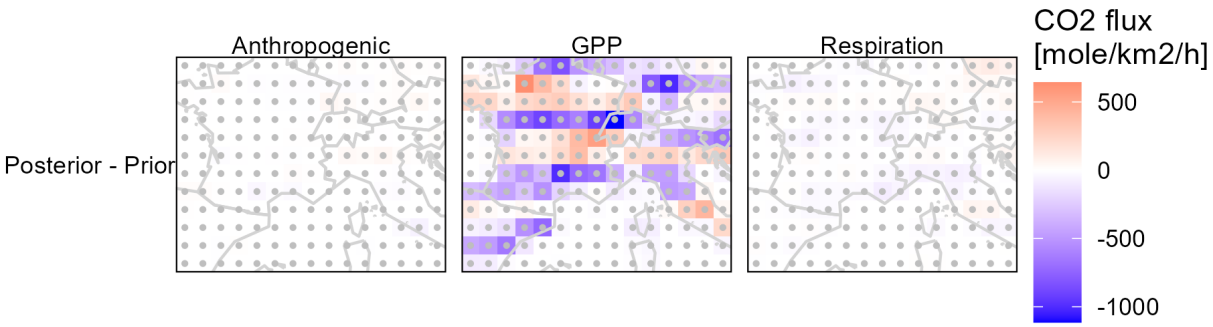

Figure 4.1.2.3: Same as Figure 4.1.2.1, but with the bug that also affected the results in Section 4.1.

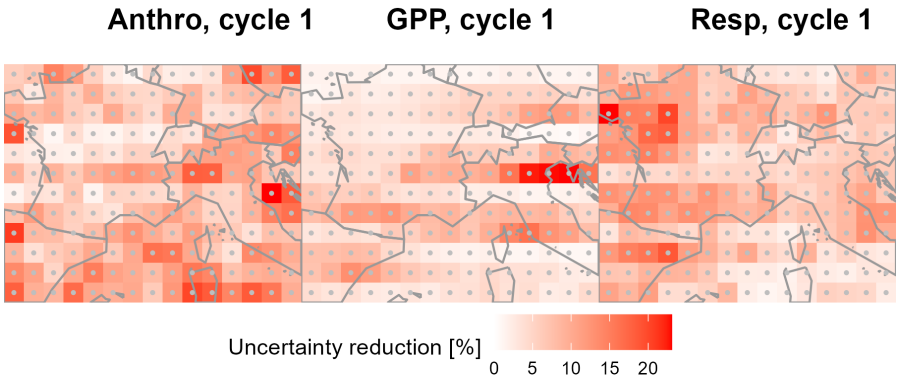

Figure 4.1.2.4: Same as Figure 4.1.2.2, but with the bug that also affected the results in Section 4.1.

4.1.3 LSCE

The first tests of OSSEs conducted with the CIF-CHIMERE inversions assimilating OCO-2 and surface data tend to confirm the general conclusions from the experiments using real data in T4.4 and documented in D4.6, i.e., that when using the existing observations:

- there is a lack of correction of the CO2 anthropogenic emissions.
- the assimilation of the data from existing surface network tend to better constrain the control of the CO2 terrestrial ecosystem fluxes than the assimilation of the OCO-2 data.

However, these first tests needed further analysis, and the lack of comparable OSSEs with pseudo CO2M data prevents from stating whether this mission would provide a better constraint on the CO_2 anthropogenic emissions when using a 10 km resolution inversion system, and a better constraint than the surface data for the control of the CO_2 natural fluxes.

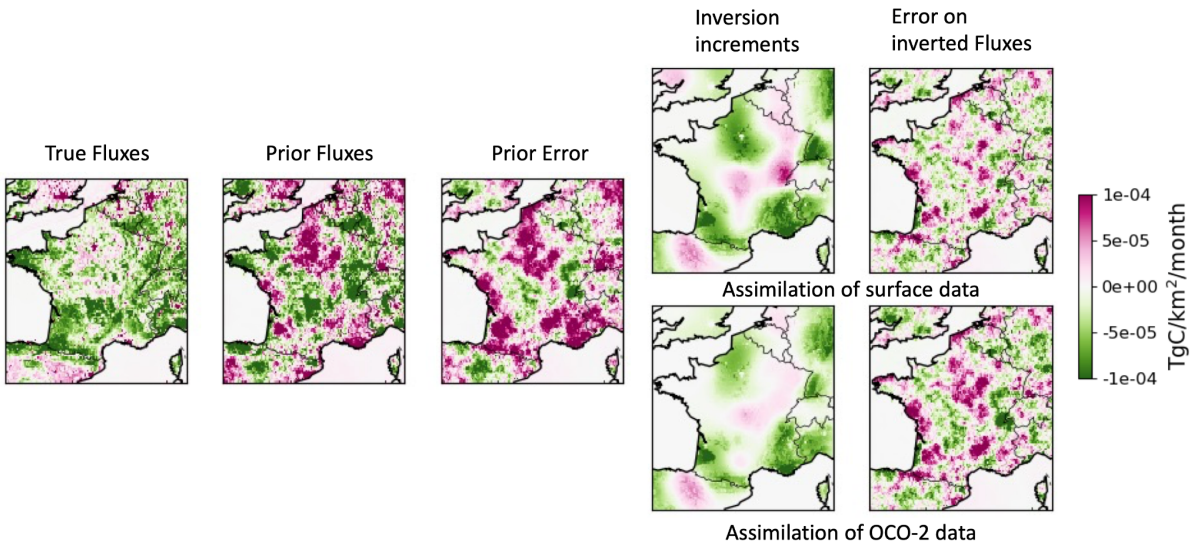

Figure 4.1.3.1: Total (anthropogenic and land biogenic) CO_2 fluxes in France in July 2018 in the first tests of OSSEs with CIF-CHIMERE assimilating surface and OCO-2 pseudo-observations.

5 Conclusion

This report documents the development work that was done in Task 5.4 to prepare regional inverse modelling systems for estimating CO_2 fluxes from European countries for the launch of the Copernicus CO2M mission. A pseudo dataset for a three-satellite configuration of the CO2M mission was made for the year 2018, to test the performance of regional inversions over Europe to evaluate and improve existing estimates of anthropogenic and biological surface fluxes that are used as a priori. Observing System Simulation Experiment (OSSE) frameworks have been designed to test the capacity of the inversions to recover 'true' fluxes from a CO_2 nature run using CO2M data or to propagate the corresponding retrieval uncertainties to the flux inversion estimates. The setups of these frameworks, experiments and datasets that were used are described in this document. The OSSE setup allows investigating the impact of heterogeneous samples due to cloud cover, by redistributing the number of valid retrievals randomly across the satellite orbits.
Inversions were performed following the OSSE protocol and first results are shown for the WRF-CTDAS and CIF-Chimere inversion systems. Some obvious shortcomings remain in the results due to a bug in WRF-CTDAS code developed for CoCO2 that was identified late. The bug fix was demonstrated with a numerically small test case, but the time that remained for repeating all simulations was too short. For this reason, the main outcome from T5.4 and this deliverable is the progress that was made in CoCO2 to develop and test inversion systems, which is valuable in view of the launch of CO2M in 2026. Conclusions regarding the performance of regional inversions using CO2M data for estimating national CO_2 emissions and how it compares to the use of data from OCO-2 and the surface network can unfortunately not been drawn at this stage yet.

6 References

Agustí-Panareda, A., McNorton, J., Balsamo, G. *et al.* Global nature run data with realistic high-resolution carbon weather for the year of the Paris Agreement. *Sci Data* 9, 160 (2022). https://doi.org/10.1038/s41597-022-01228-2

Beck, V., T. Koch, R. Kretschmer, J. Marshall, R. Ahmadov, C. Gerbig, D. Pillai, and M. Heimann, (2011): The WRF Greenhouse Gas Model (WRF-GHG). Technical Report No. 25, Max Planck Institute for Biogeochemistry, Jena, Germany.

Berchet, A., Sollum, E., Thompson, R. L., Pison, I., Thanwerdas, J., Broquet, G., Chevallier, F., Aalto, T., Berchet, A., Bergamaschi, P., Brunner, D., Engelen, R., Fortems-Cheiney, A., Gerbig, C., Groot Zwaaftink, C. D., Haussaire, J.-M., Henne, S., Houweling, S., Karstens, U., Kutsch, W. L., Luijkx, I. T., Monteil, G., Palmer, P. I., van Peet, J. C. A., Peters, W., Peylin, P., Potier, E., Rödenbeck, C., Saunois, M., Scholze, M., Tsuruta, A., and Zhao, Y.: The Community Inversion Framework v1.0: a unified system for atmospheric inversion studies, Geosci. Model Dev., 14, 5331–5354, https://doi.org/10.5194/gmd-14-5331-2021, 2021.

Boesch, H.; Baker, D.; Connor, B.; Crisp, D.; Miller, C. Global Characterization of CO_2 Column Retrievals from Shortwave-Infrared Satellite Observations of the Orbiting Carbon Observatory-2 Mission. *Remote Sens.* **2011**, *3*, 270-304. https://doi.org/10.3390/rs3020270

Broquet, G., Chevallier, F., Bréon, F.-M., Kadygrov, N., Alemanno, M., Apadula, F., Hammer, S., Haszpra, L., Meinhardt, F., Morguí, J. A., Necki, J., Piacentino, S., Ramonet, M., Schmidt, M., Thompson, R. L., Vermeulen, A. T., Yver, C., and Ciais, P.: Regional inversion of CO2 ecosystem fluxes from atmospheric measurements: reliability of the uncertainty estimates, Atmos. Chem. Phys., 13, 9039–9056, https://doi.org/10.5194/acp-13-9039-2013, 2013.

Buchwitz, M., Reuter, M., Bovensmann, H., Pillai, D., Heymann, J., Schneising, O., Rozanov, V., Krings, T., Burrows, J. P., Boesch, H., Gerbig, C., Meijer, Y., and Löscher, A.: Carbon Monitoring Satellite (CarbonSat): assessment of atmospheric CO2 and CH4 retrieval errors by error parameterization, Atmos. Meas. Tech., 6, 3477–3500, https://doi.org/10.5194/amt-6-3477-2013, 2013.

Denier van der Gon et al., CoCO2 Deliverable 2.1, https://coco2-project.eu/sites/default/files/2022-03/CoCO2-D2.1-V1-0.pdf

ESA Earth and Mission Science Division, (2020). Tech. rep. Version 3.0. Copernicus CO2 Monitoring Mission Requirements Document (MRD), Available at: https://esamultimedia.esa.int/docs/EarthObservation/CO2M_MRD_v3.0_20201001_Issued.pdf. (Access:1 February 2023).

Fortems-Cheiney, A., Pison, I., Broquet, G., Dufour, G., Berchet, A., Potier, E., Coman, A., Siour, G., and Costantino, L.: Variational regional inverse modeling of reactive species emissions with PYVAR-CHIMERE-v2019, Geosci. Model Dev., 14, 2939–2957, https://doi.org/10.5194/gmd-14-2939-2021, 2021.

Grell, G. A., Peckham, S. E., Schmitz, R., McKeen, S. A., Frost, G., Skamarock, W. C., & Eder, B. (2005). Fully coupled “online” chemistry within the wrf model. Atmospheric Environment, 39 (37), 6957–6975

Hersbach, H. et al. (2017) Complete ERA5 from 1940: Fifth generation of ECMWF atmospheric reanalyses of the global climate. Copernicus Climate Change Service (C3S) Data Store (CDS), DOI:10.24381/cds.143582cf

Hersbach, H., Bell, B., Berrisford, P., Biavati, G., Horányi, A., Muñoz Sabater, J., Nicolas, J., Peubey, C., Radu, R., Rozum, I., Schepers, D., Simmons, A., Soci, C., Dee, D., Thépaut, J-N. (2023a): ERA5 hourly data on single levels from 1940 to present. Copernicus Climate Change Service (C3S) Climate Data Store (CDS), DOI: 10.24381/cds.adbb2d47 (Accessed on 15-04-2023)

Hersbach, H., Bell, B., Berrisford, P., Biavati, G., Horányi, A., Muñoz Sabater, J., Nicolas, J., Peubey, C., Radu, R., Rozum, I., Schepers, D., Simmons, A., Soci, C., Dee, D., Thépaut, J-N. (2023b): ERA5 hourly data on pressure levels from 1940 to present. Copernicus Climate Change Service (C3S) Climate Data Store (CDS), DOI: 10.24381/cds.bd0915c6 (Accessed on 15-04-2023)

Inness, A., Ades, M., Agustí-Panareda, A., Barré, J., Benedictow, A., Blechschmidt, A.-M., Dominguez, J. J., Engelen, R., Eskes, H., Flemming, J., Huijnen, V., Jones, L., Kipling, Z., Massart, S., Parrington, M., Peuch, V.-H., Razinger, M., Remy, S., Schulz, M., and Suttie, M.: The CAMS reanalysis of atmospheric composition, Atmos. Chem. Phys., 19, 3515–3556, https://doi.org/10.5194/acp-19-3515-2019, 2019.

Kaminski T, Scholze M, Rayner P, Houweling S, Voßbeck M, Silver J, Lama S, Buchwitz M, Reuter M, Knorr W, Chen HW, Kuhlmann G, Brunner D, Dellaert S, Denier van der Gon H, Super I, Löscher A and Meijer Y (2022) Assessing the Impact of Atmospheric CO2 and NO2 Measurements From Space on Estimating City-Scale Fossil Fuel CO2 Emissions in a Data Assimilation System. Front. Remote Sens. 3:887456. doi: 10.3389/frsen.2022.887456

Kuhlmann G, Henne S, Meijer Y and Brunner D (2021) Quantifying CO2 Emissions of Power Plants With CO2 and NO2 Imaging Satellites. Front. Remote Sens. 2:689838. doi: 10.3389/frsen.2021.689838.

Lu S, Landgraf J, Fu G, van Diedenhoven B, Wu L, Rusli SP and Hasekamp OP (2022) Simultaneous Retrieval of Trace Gases, Aerosols, and Cirrus Using RemoTAP—The Global Orbit Ensemble Study for the CO2M Mission. Front. Remote Sens. 3:914378. doi: 10.3389/frsen.2022.914378.

McGrath, M. J., Petrescu, A. M. R., Peylin, P., Andrew, R. M., Matthews, B., Dentener, F., Balkovič, J., Bastrikov, V., Becker, M., Broquet, G., Ciais, P., Fortems-Cheiney, A., Ganzenmüller, R., Grassi, G., Harris, I., Jones, M., Knauer, J., Kuhnert, M., Monteil, G., Munassar, S., Palmer, P. I., Peters, G. P., Qiu, C., Schelhaas, M.-J., Tarasova, O., Vizzarri, M., Winkler, K., Balsamo, G., Berchet, A., Briggs, P., Brockmann, P., Chevallier, F., Conchedda, G., Crippa, M., Dellaert, S. N. C., Denier van der Gon, H. A. C., Filipek, S., Friedlingstein, P., Fuchs, R., Gauss, M., Gerbig, C., Guizzardi, D., Günther, D., Houghton, R. A., Janssens-Maenhout, G., Lauerwald, R., Lerink, B., Luijkx, I. T., Moulas, G., Muntean, M., Nabuurs, G.-J., Paquirissamy, A., Perugini, L., Peters, W., Pilli, R., Pongratz, J., Regnier, P., Scholze, M., Serengil, Y., Smith, P., Solazzo, E., Thompson, R. L., Tubiello, F. N., Vesala, T., and Walther, S.: The consolidated European synthesis of CO2 emissions and removals for the European Union and United Kingdom: 1990–2020, Earth Syst. Sci. Data, 15, 4295–4370, https://doi.org/10.5194/essd-15-4295-2023, 2023.

Menut, L., Bessagnet, B., Khvorostyanov, D., Beekmann, M., Blond, N., Colette, A., Coll, I., Curci, G., Foret, G., Hodzic, A., Mailler, S., Meleux, F., Monge, J.-L., Pison, I., Siour, G., Turquety, S., Valari, M., Vautard, R., and Vivanco, M. G.: CHIMERE 2013: a model for regional

atmospheric composition modelling, Geosci. Model Dev., 6, 981–1028, https://doi.org/10.5194/gmd-6-981-2013, 2013.

Monteil, G., Broquet, G., Scholze, M., Lang, M., Karstens, U., Gerbig, C., Koch, F.-T., Smith, N. E., Thompson, R. L., Luijkx, I. T., White, E., Meesters, A., Ciais, P., Ganesan, A. L., Manning, A., Mischurow, M., Peters, W., Peylin, P., Tarniewicz, J., Rigby, M., Rödenbeck, C., Vermeulen, A., and Walton, E. M.: The regional European atmospheric transport inversion comparison, EUROCOM: first results on European-wide terrestrial carbon fluxes for the period 2006–2015, Atmos. Chem. Phys., 20, 12063–12091, https://doi.org/10.5194/acp-20-12063-2020, 2020.

Peters, W., Miller, J. B., Whitaker, J. S., Denning, A. S., Hirsch, A., Krol, M. C., et al. (2005). An ensemble data assimilation system to estimate CO2 surface fluxes from atmospheric trace gas observations. Journal of Geophysical Research Atmospheres, 110(24), 1–18. https://doi.org/10.1029/2005JD006157

Potier, E., Broquet, G., Wang, Y., Santaren, D., Berchet, A., Pison, I., Marshall, J., Ciais, P., Bréon, F.-M., and Chevallier, F.: Complementing XCO2 imagery with ground-based CO2 and 14CO2 measurements to monitor CO2 emissions from fossil fuels on a regional to local scale, Atmos. Meas. Tech., 15, 5261–5288, https://doi.org/10.5194/amt-15-5261-2022, 2022.

Rossow, W.B.; Walker, A.; Golea, V.; Knapp, K. R.; Young, A.; Inamdar A.; Hankins, B.; and NOAA's Climate Data Record Program (2016): International Satellite Cloud Climatology Project Climate Data Record, H-Series [indicate subset used] NOAA National Centers for Environmental Information. [access date]. doi:10.7289/V5QZ281S

Rusli, S. P., Hasekamp, O., aan de Brugh, J., Fu, G., Meijer, Y., and Landgraf, J. (2021). Anthropogenic CO2 Monitoring Satellite mission: the Need for Multi- Angle Polarimetric Observations. Atmos. Meas. Tech. 14, 1167–1190. doi:10.5194/amt-14-1167-2021.

Sierk,B.Bézy,J.-L.,Loscher,A.,and Meijer,Y.(2019).TheEuropeanCO2 Monitoring Mission: Observing Anthropogenic Greenhouse Gas Emissions from Space 11180. Proceedings, International Conference on Space Optics — ICSO 2018. 12 July 2019. Chania, Greece. 111800M. doi:10.1117/12.2535941.

Skamarock, W. C., J. B. Klemp, J. Dudhia, D. O. Gill, Z. Liu, J. Berner, W. Wang, J. G. Powers, M. G. Duda, D. M. Barker, and X.-Y. Huang, 2019: A Description of the Advanced Research WRF Version 4. NCAR Tech. Note NCAR/TN-556+STR, 145 pp. doi:10.5065/1dfh-6p97

Super, I., Dellaert, S. N. C., Visschedijk, A. J. H., and Denier van der Gon, H. A. C.: Uncertainty analysis of a European high-resolution emission inventory of CO2 and CO to support inverse modelling and network design, Atmos. Chem. Phys., 20, 1795–1816, https://doi.org/10.5194/acp-20-1795-2020, 2020.

Technical Note for ESA study: LOGOFLUX 2- CarbonSat Earth Explorer 8 Candidate Mission - Inverse Modelling and Mission Performance Study, Michael Buchwitz, 2014 (NOV-7248-NT-4080).

van Der Laan-Luijkx, I. T., Van Der Velde, I. R., Van Der Veen, E., Tsuruta, A., Stanislawska, K., Babenhauserheide, A., Fang Zhang, H., Liu, Y., He, W., Chen, H., Masarie, K. A., Krol, M. C. and Peters, W.: The CarbonTracker Data Assimilation Shell (CTDAS) v1.0: Implementation and global carbon balance 2001-2015, Geosci. Model Dev., 10(7), 2785–2800, doi:10.5194/gmd-10-2785- 2017, 2017.

Wang, Y., Broquet, G., Bréon, F.-M., Lespinas, F., Buchwitz, M., Reuter, M., Meijer, Y., Loescher, A., Janssens-Maenhout, G., Zheng, B., and Ciais, P.: PMIF v1.0: assessing the potential of satellite observations to constrain CO2 emissions from large cities and point sources over the globe using synthetic data, Geosci. Model Dev., 13, 5813–5831, https://doi.org/10.5194/gmd-13-5813-2020, 2020.

Document History

Version	Author(s)	Date	Changes
	Name (Organisation)	dd/mm/yyyy	
1	VUA	20/12/2023	First version for submission

Internal Review History

Internal Reviewers	Date	Comments
Name (Organisation)	dd/mm/yyyy	

Estimated Effort Contribution per Partner

Partner	Effort
VUA	14
Total	**14**